Journal of Materials Chemistry A

ROYAL SOCIETY OF CHEMISTRY

PAPER

View Article Online
View Journal | View Issue

Check for updates

Cite this: J. Mater. Chem. A, 2023, 11, 4769

A multifunctional paper-based supercapacitor with excellent temperature adaptability, plasticity, tensile strength, self-healing, and high thermoelectric effects†

Chuanyin Xiong, *[a] Qi Yang,[a] Weihua Dang,[a] Qiusheng Zhou,[a] Xue Jiang,[a] Xuhui Sun,[b] Zequn Wang,[b] Meng An*[b] and Yonghao Ni[c]

In recent years, the development of multi-functional supercapacitors with high flexibility and strong environmental adaptability has gradually become a focus of attention. In this work, a multi-functional paper-based supercapacitor with excellent temperature adaptability, plasticity, tensile strength, strong adhesion, and self-healing properties is obtained by introducing PVA and $ZnCl_2$ into carbonized paper-based materials (APC-PVA@$ZnCl_2$). The as-obtained APC-PVA@$ZnCl_2$ supercapacitor has excellent adaptability to the environment, even in a low-temperature environment below zero, still maintaining a high volumetric specific capacitance of 3438.45 mF cm^{-3} and high volumetric specific energy density of 44 mW h cm^{-3}. Moreover, the APC-PVA@$ZnCl_2$ supercapacitor can be stretched beyond 2400–2500% strain, indicating good tensile properties. In addition, the APC-PVA@$ZnCl_2$ composite can also be used as a sensing material to detect current signals with different characteristics generated by the movement of different parts of the human body, showing excellent sensing performance. Besides, the APC-PVA@$ZnCl_2$ composite also displays outstanding thermoelectric properties. It is hoped that this work can provide a reference for the development of green multi-functional supercapacitors.

Received 29th November 2022
Accepted 1st February 2023

DOI: 10.1039/d2ta09654d

rsc.li/materials-a

Published on 02 února 2023. Downloaded on 19.04.2026 21:13:25.

1. Introduction

Energy and environmental issues have always been two key core issues that cannot be avoided in the development of human society.[1–5] Especially with the continuous reduction of petrochemical resources and outstanding environmental problems caused by them, researchers have been focussing on the research and development of new and sustainable green electrochemical energy sources.[6–10] Among them, supercapacitors, as electrochemical energy storage devices with high power density, long cycle life, good safety, and other advantages, have attracted extensive attention from researchers.[11–16] Although the comprehensive electrochemical storage performance of supercapacitors has made great progress after decades of development, there are still some key problems to be studied further as follows: (1) as we all know, electrode materials, as one of the key factors affecting energy storage devices, have always been an important aspect of researchers' attention and improvement and various types of electrode materials are also available. However, electrode materials that can truly give green, sustainable, and high performance are still limited. (2) Recently, with the rapid development of flexible wearable devices, people have been increasingly having high requirements for a comprehensive performance of energy storage devices, such as good environmental adaptability, excellent flexibility, good mechanical properties, plasticity, and self-healing ability, not just limited to energy storage characteristics. Incorporating these excellent performances into integrated energy storage devices still has certain challenges.

In recent years, as a green, sustainable, widely sourced, and naturally rich porous structural material, biomass materials are increasingly favored by researchers in the field of electrochemical energy storage,[17–22] providing a further feasible idea to solve the above-mentioned key problems. Among them, paper-based materials, as a derivative product derived from biomass materials, not only have some advantages of biomass materials but also have good flexibility and integrity with potential as excellent energy storage materials.[23–26] Many researchers have used paper-based materials for energy storage research and have also achieved a series of good research results. Currently, paper-based materials are used as flexible substrates in the field

[a]College of Bioresources Chemical & Materials Engineering, Shaanxi University of Science and Technology, Xi'an 710021, China. E-mail: xiongchuanyin@126.com; xiongchuanyin@sust.edu.cn

[b]College of Mechanical and Electrical Engineering, Shaanxi University of Science & Technology, Xi'an 710021, China. E-mail: anmeng@sust.edu.cn

[c]Department of Chemical and Biomedical Engineering, University of Maine, Orono, Maine, 04469, USA

† Electronic supplementary information (ESI) available. See DOI: https://doi.org/10.1039/d2ta09654d

Published on 02 února 2023. Downloaded on 19.04.2026 21:13:25.

of energy storage.[27–29] However, paper-based materials are derived from biomass materials and poor conductivity is still an unavoidable disadvantage. Therefore, the carbonization treatment of biomass materials is an effective strategy to improve its conductivity and has been widely adopted by researchers. It is true that carbonization treatment can effectively improve the conductivity of biomass materials, but the flexibility, mechanical strength, and environmental adaptability of carbonized materials are seriously affected.

Based on these challenges mentioned above, in this research, for the first time, by introducing PVA and $ZnCl_2$ into carbonized paper-based materials (APC-PVA@$ZnCl_2$), using the cross-linked network structure formed by PVA, $ZnCl_2$, and paper-based materials and the interaction between Zn^{2+}, PVA, and paper-based fibers, a multi-functional paper-based supercapacitor with excellent temperature adaptability, plasticity, super-tensile, strong adhesion and self-healing properties is obtained. Furthermore, the interaction between PVA, $ZnCl_2$, and paper fibers was simulated by molecular dynamics, which confirmed the experimental results. Finally, for the as-obtained APC-PVA@$ZnCl_2$ supercapacitor, high specific capacitances of 3438.45 and 8176.94 mF cm^{-3} were still obtained at a scan rate of 50 mV s^{-1} at −5 °C and 80 °C at a scan rate of 50 mV s^{-1}, respectively. The volumetric energy density is up to 44 mW h cm^{-3}. These electrochemical properties prove its strong adaptability in different environments. Moreover, the APC-PVA@$ZnCl_2$ supercapacitor can be stretched beyond 2400–2500% strain, proving they have good tensile properties. Besides, the APC-PVA@$ZnCl_2$ multi-functional composite can also be used as a sensing material to detect current signals with different characteristics generated by the movement of different parts of the human body, showing excellent sensing performance. In addition, the APC-PVA@$ZnCl_2$ multi-functional composite also shows a sparkling thermoelectric effect. Finally, molecular dynamics simulation and density functional theory are used to study the effect of material structures and functional groups on the diffusion of Zn^{2+}. In a word, this research work provides new ideas and feasible references for the above-mentioned challenging problems in the field of energy storage.

2. Experiments section

Fig. 1 shows the schematic diagram of fabricating versatile integrated paper-based functional materials with good plasticity based on carbonized paper-based materials. The specific preparation details and relevant test methods are displayed in the ESI.† Here, TP represents tissue paper, and APC is carbonized activated paper carbon.

3. Results and discussion

3.1. Structure and morphology

For the carbonized paper-based materials, Fig. 2a–c show the SEM images of activated paper carbon (APC) under different magnifications. At higher magnification, it can be seen that the morphology of crude fibers still exists after the carbonization of paper-based material (Fig. 2a and b), at a lower magnification, it can be seen that the carbonized paper still retains the hierarchical network structure of the original paper (Fig. 2c). This not only increases the effective loading and stability of the active material but also improves the effective penetration depth of electrolyte into the paper-based active layer, thus significantly increasing the energy density of APC. Fig. 2d–f are SEM images of carbonized paper soaked in PVA solution (APC@PVA) under different magnifications. It can be seen that the PVA solution is

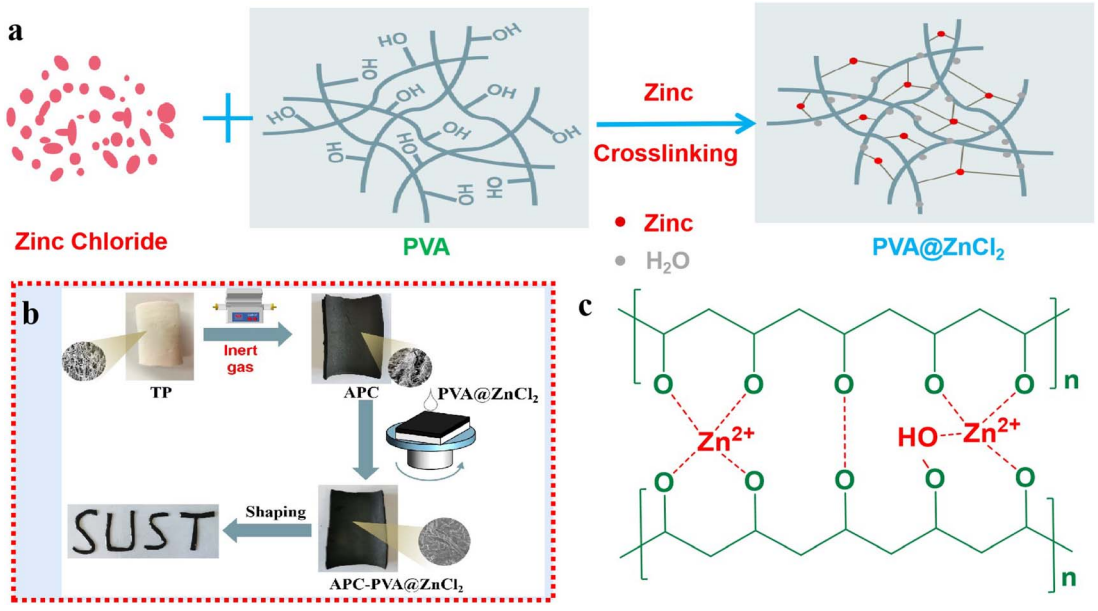

Fig. 1 (a) Configuration mechanism of PVA@$ZnCl_2$ solution. (b) The preparation process of APC-PVA@$ZnCl_2$ with good plasticity. (c) The cross-linking mechanism between PVA and Zn^{2+}.

 This journal is © The Royal Society of Chemistry 2023

Published on 02 února 2023. Downloaded on 19.04.2026 21:13:25.

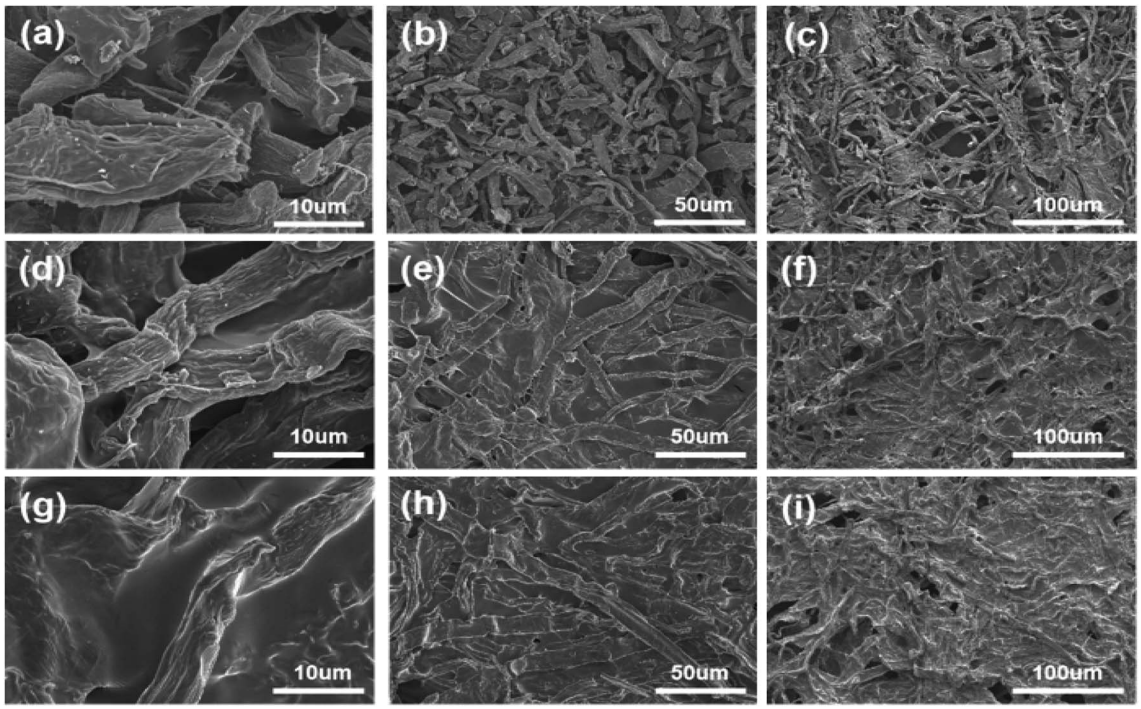

Fig. 2 The SEM images of (a–c) APC, (d–f) APC@PVA, (g–i) APC-PVA@$ZnCl_2$ under different magnifications.

tightly coated on the surface of the carbon fiber (Fig. 2d and e). Moreover, the layered porous structure of the paper base can provide more channels for electrolyte ions to transport, and the PVA solution can be well immersed into the layered porous structure of APC. Fig. 2g–i show the SEM images of carbonized paper soaked in PVA@$ZnCl_2$ solution (APC-PVA@$ZnCl_2$) under different magnifications. Compared with the SEM images of the APC@PVA composite, it can be found that the pore size of APC-PVA@$ZnCl_2$ is smaller, and the cross-linking structure is complete, indicating that the PVA@$ZnCl_2$ solution almost covers every carbon fiber.

Furthermore, the composition of the paper-based material is further determined by infrared spectra, as shown in the Fig. S1 of the ESI.† Fig. S1† displays the infrared patterns of APC, APC@PVA, and APC-PVA@$ZnCl_2$ samples. For the APC@PVA sample, the characteristic bands of 3388 cm^{-1} and 2928 cm^{-1} belong to the stretching vibration of the O–H and C–H groups, respectively. The peaks at 1636, 1380, 1075, 830, and 522 cm^{-1} are attributed to O–H bending vibration, symmetric –CH_2– bending vibration, C–O tensile vibration, and C–C tensile vibration, respectively.[30,31] For APC-PVA@$ZnCl_2$ samples, there are similar bar graphs, but the positions are slightly different. Compared with APC@PVA, the vibration peak caused by O–H stretching and bending is significantly increased. Moreover, C–O and C–C group stretching vibrations not only increase the peak value but also have a more obvious red shift.[26,32] This is because the coordination of Zn^{2+} and the reduction of water content promote the interaction between PVA chains in the amorphous region.[33]

3.2. Electrochemical performance

3.2.1 APC-PVA@$ZnCl_2$ integrated paper-based supercapacitor. The tolerance of APC-PVA@$ZnCl_2$ supercapacitor to different ambient temperatures, especially the adaptability to high and low-temperature environments, is investigated. Herein, high temperature (80 °C), low temperature (−5 °C), and room temperature (25 °C) conditions are selected to study and compare the electrochemical performance of APC-PVA@$ZnCl_2$ supercapacitor under different potential windows (0–0.8 V, 0–1 V, and 0–1.6 V) and various scan rates (10–100 mV s^{-1}), as shown in Fig. 3 and S2.† Through the above CV electrochemical test results, the following conclusions are obtained: (1) for all CV curves, irrespective of the temperature, potential window, or scan rates, all CV curves of APC-PVA@$ZnCl_2$ supercapacitor show obvious redox peak, and the potential window is significantly increased up to 1.6 V due to the presence of Zn^{2+} gel electrolyte. Moreover, we also checked the GCD curves of the sample under different current densities and different temperatures under the 0–1.6 V potential window (Fig. S3†). Obviously, the GCD curves under these conditions show the characteristics of nonlinear change, suggesting the existence of pseudocapacitance, which is consistent with the results of the above CV curves. (2) Under different temperatures and scan rates, all CV curves show an approximately rectangular shape, suggesting good capacitive characteristics and electrochemical stability. Furthermore, at a scan rate of 50 mV s^{-1}, the APC-PVA@$ZnCl_2$ supercapacitor shows approximately consistent trends of change under different ambient temperatures and various potential windows, further implying that the APC-

Published on 02 února 2023. Downloaded on 19.04.2026 21:13:25.

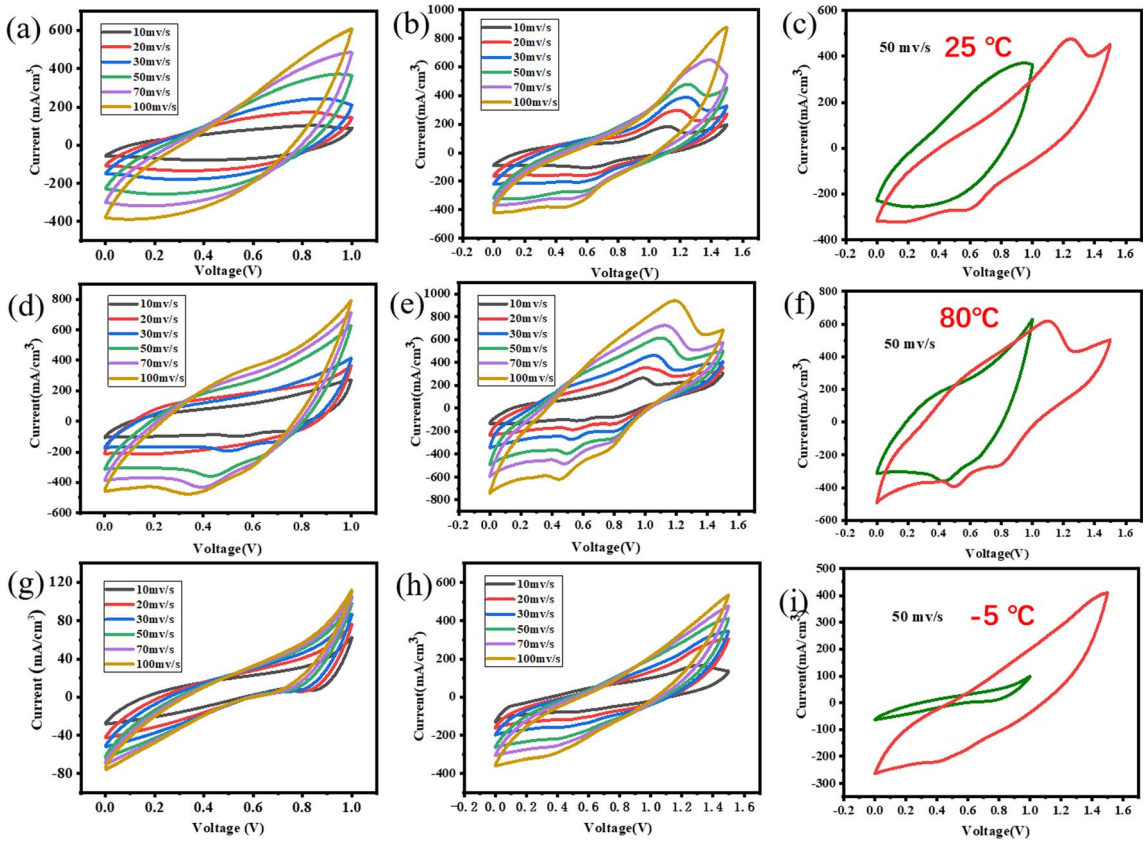

Fig. 3 (a, d and g) Typical CV curves of APC-PVA@$ZnCl_2$ at different temperatures between the potential range of 0 and 1 V and at different scanning rates, (b, e and h) Typical CV curves of APC-PVA@$ZnCl_2$ with different scanning rates between the potential range of 0 and 1.6 V at different temperatures, (c, f and i) CV contrast diagram under various potential windows at different temperatures at a scan rate of 50 mV s^{-1}.

PVA@$ZnCl_2$ supercapacitor has good electrochemical stability at different ambient temperatures. In addition, through calculations, it is found that at room temperature (25 °C), higher volumetric specific capacitances of 5764.48 mF cm^{-3} and 5277.58 mF cm^{-3} are obtained at 0–1 V and 0–1.6 V potential windows, respectively (Fig. 3c). More excitedly, when the outside temperature rises to 80 °C, the volumetric specific capacitances of the APC-PVA@$ZnCl_2$ supercapacitor are even higher up to 7550.96 mF cm^{-3} and 8176.94 mF cm^{-3}, respectively, at the same condition (Fig. 3f). This is because the rise in temperature accelerates the flow of electrolyte ions in the APC-PVA@$ZnCl_2$ supercapacitor, which enables more electrolyte ions to reach the interior of the electrode material bulk phase, thus effectively improving the specific capacitance of the supercapacitor. On the whole, these volumetric specific capacitance values can be compared to some previous literature works,[34–37] as displayed in Fig. 4c. More importantly, when the temperature drops to −5 °C, APC-PVA@$ZnCl_2$ supercapacitor can still maintain high volumetric specific capacitances of 562.70 mF cm^{-3} and 3438.45 mF cm^{-3}, respectively, as shown in Fig. 3i, which is 68% of the specific capacitance at room temperature, showing the applicability of the supercapacitor in cold regions. This is due to the coordination effect of Zn^{2+} and the weakening of hydrogen bonding force at a low temperature, which makes the APC-PVA@$ZnCl_2$ supercapacitor still have a high specific capacity. Moreover, the volumetric energy density is as high as 44 mW h cm^{-3}. These electrochemical values above are comparable with that of some outstanding works in recent years,[38–42] as shown in Fig. 4d. Furthermore, the corresponding Nyquist diagram of the APC-PVA@$ZnCl_2$ supercapacitor is investigated, as shown in Fig. S2f of the ESI.† The inclined line in the low-frequency region corresponds to the diffusion of electrolyte ions on the surface and inside. It can be seen that the APC-PVA@$ZnCl_2$ supercapacitor shows a lower charge transfer resistance (R_{CT}) of approximately 25 Ω. In the cyclic test, R_{CT} can be ignored, the slope can also be ignored, and the angle becomes larger at low frequency, indicating that the electrochemical kinetic cycle is longer, which is conducive to charge transfer and storage. In addition, the CV curves of the APC-PVA@$ZnCl_2$ supercapacitor under different temperature conditions with a scan rate of 50 mV s^{-1} and typical GCD curves under different temperature conditions and various current densities are exhibited in Fig. S4 of the ESI.† The results further support the above conclusions. It is found that the absolute area of CV curves of the APC-PVA@$ZnCl_2$ supercapacitor increases significantly with the increase in temperature, implying the increase in specific capacitance. Also, at a low temperature, the APC-PVA@$ZnCl_2$ supercapacitor still shows a larger absolute area of CV curve, indicating that a higher specific capacitance is still maintained. All of these results are consistent with the above

 This journal is © The Royal Society of Chemistry 2023

Published on 02 února 2023. Downloaded on 19.04.2026 21:13:25.

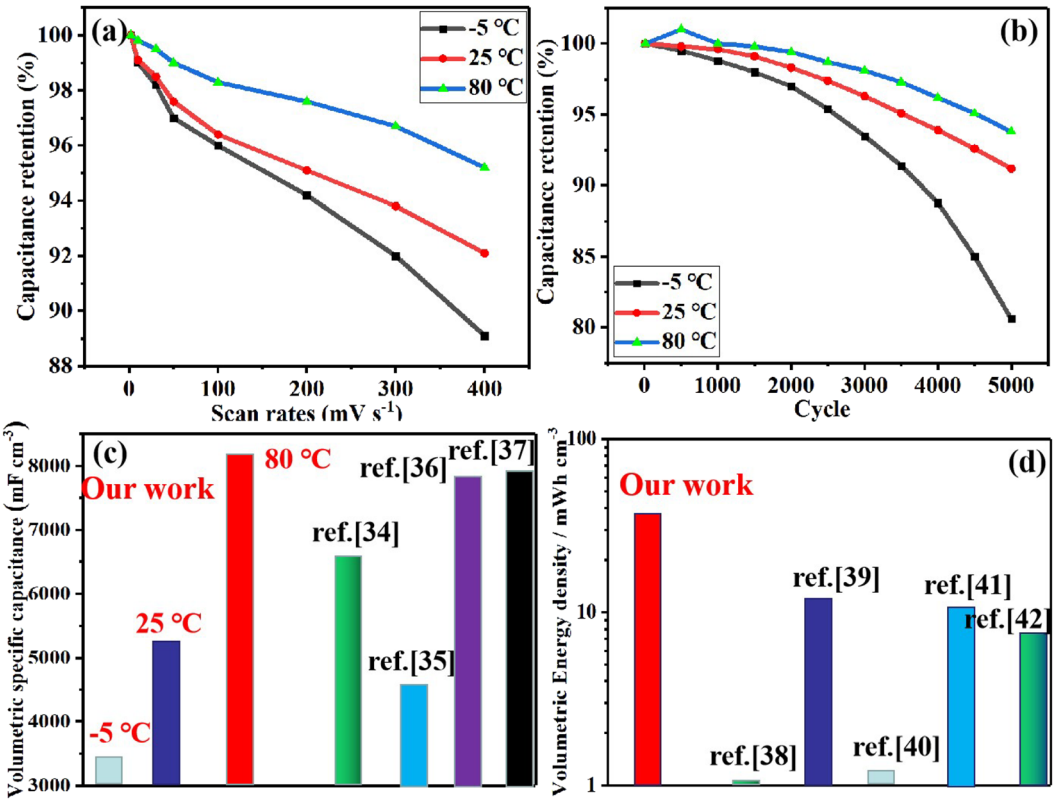

Fig. 4 (a) Capacitance retention of APC-PVA@$ZnCl_2$ (a) at different temperatures and scan rates. (b) After experiencing 5000 cycles. (c and d) Comparison maps of volumetric specific capacitance and energy density of APC-PVA@$ZnCl_2$ with reported work.

electrochemical analysis results. In addition, rate performance is also an important parameter. Fig. 4a shows the change in capacitance retention of APC-PVA@$ZnCl_2$ samples under various temperatures at different scan rates. Obviously, at different scan rates, even in a higher scan rate, all the APC-PVA@$ZnCl_2$ samples under various temperatures display a capacitance retention of more than 88%, which demonstrates that APC-PVA@$ZnCl_2$ samples have excellent rate performance at different ambient temperatures. Furthermore, Fig. 4b displays the change of capacitance retention of APC-PVA@$ZnCl_2$ samples under various temperatures after experiencing 5000 cycles. It can be seen that the capacitance retention rate of samples at different temperatures is maintained above 80%, suggesting that the samples have good stability in different environments. In addition, Fig. 4c and d) displays comparison maps of volumetric specific capacitance and energy density of APC-PVA@$ZnCl_2$ with reported works.[34–42] It is obvious that our work can be compared with those excellent works in recent years. All in all, these results demonstrate that the APC-PVA@$ZnCl_2$ supercapacitor has excellent environmental adaptability, showing its potential application value in different environments.

3.3. Integrated APC-PVA@$ZnCl_2$ paper-based supercapacitor applied in sensor

3.3.1 Monitoring human motion. APC-PVA@$ZnCl_2$ materials exhibit strong mechanical compliance on irregularly curved skin surfaces, such as the human elbow and interphalangeal joints (Fig. 5a and b), without any retraction or delamination during testing, demonstrating their strong interface adhesion. Based on this, APC-PVA@$ZnCl_2$ materials can be fixed at different joint positions of the human body to detect changes in human physiological motion signals. Fig. 5a displays the human motion signal detected by the APC-PVA@$ZnCl_2$ composite strain sensor attached to the finger joint, which is used to detect the bending motion of the finger. Its signal sensitivity is about 300 ms as shown in Fig. S5b in the ESI.† As can be seen, the finger joint has a unique peak structure at the bend. Moreover, at the straightening point, the current signal returns to the peak bottom, and this process can be repeated. The results show that the sensor can detect repetitive signals in the process of fingertip bending and stretching. Furthermore, when the fingertips are bent to the same extent, the same electrical signals are generated. Fig. 5b shows an electrical signal caused by elbow bending, and the electrical signal sensitivity is about 520 ms (Fig. S5c in the ESI†). The peak structure is similar to that caused by fingertip bending. Moreover, no residue or allergy on the skin was observed after the APC-PVA@$ZnCl_2$ composite was attached for 12 h. Furthermore, the dynamic signal change of the APC-PVA@$ZnCl_2$ composite during the stretching process under different states was detected, as shown in Fig. 5c. It is found that the signal increases gradually with the increase in stretching length. Finally, when the APC-PVA@$ZnCl_2$ composite material broke,

Published on 02 února 2023. Downloaded on 19.04.2026 21:13:25.

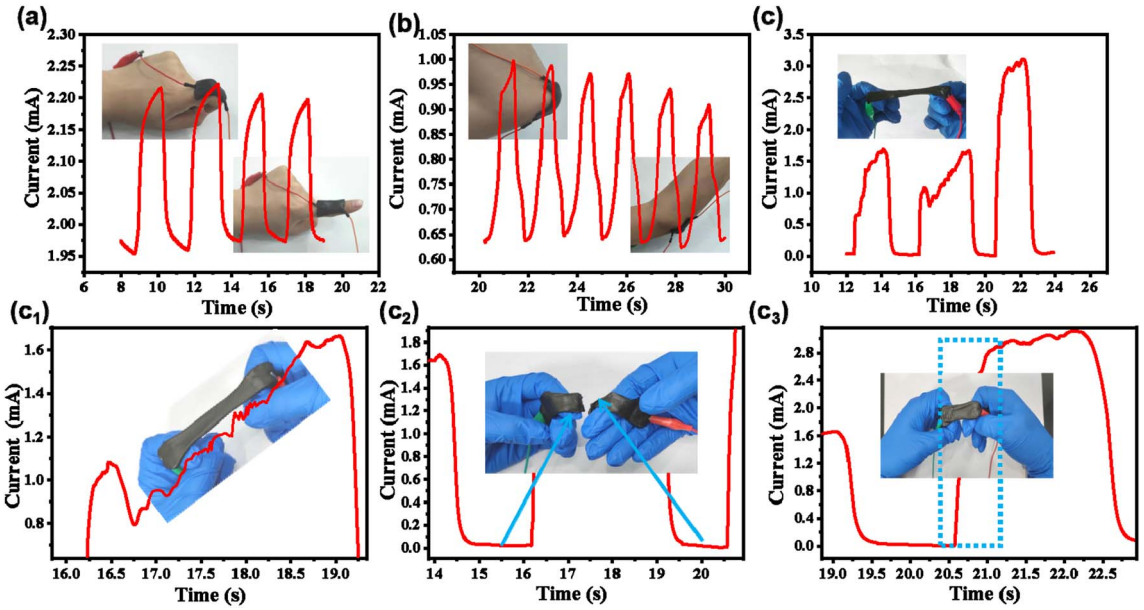

Fig. 5 Monitoring the changes of electrical signals during (a) finger and (b) elbow movements and (c–c_3) material stretching under different tensile conditions based on the APC-PVA@$ZnCl_2$ sensor.

instantaneously, the current signal was 0 (Fig. 5c_2). Interestingly, the two parts of the APC-PVA@$ZnCl_2$ composite fracture adhered together again, and the current signal immediately recovered (Fig. 5c_3). Moreover, it is worth noting that the APC-PVA@$ZnCl_2$ composite material has a high sensitivity in the fracture tensile sensing test. During the bonding process with a small force, the signal recovery takes only 200 ms, and the fracture signal loss takes only 400 ms (Fig. S5a in the ESI†). More importantly, the fractured APC-PVA@$ZnCl_2$ composite can be healed under the action of a small amount of external force and still has tensile sensing properties.

3.3.2 Tensile strength, adhesion test, and self-healing property. In addition, the APC-PVA@$ZnCl_2$ composite exhibits molding tensile ability and adhesion properties due to the coordination effect of Zn^{2+}, as shown in Fig. 6a. Obviously, materials with different shapes can be obtained by simple mold manufacturing (Fig. 6a). Moreover, the APC-PVA@$ZnCl_2$ composite material still has good electrical conductivity when it is shaped into different shapes. By connecting with the battery in series, the small bulb can be lit in any shape (Fig. 6b). More interestingly, as shown in Fig. 6c and e, the APC-PVA@$ZnCl_2$ composite material can be stretched to a strain of more than 2400–2500%, even at extremely low temperatures of −30 °C (see the relevant stretching videos in Fig. S6V1 in the ESI†), which proves that the APC-PVA@$ZnCl_2$ composite material has good tensile properties, high energy dissipation capacity, and strong damage resistance. In addition, the APC-PVA@$ZnCl_2$ material also has strong adhesive properties and can adhere to different materials, such as glass, metal, plastic, *etc.* (Fig. 6d). It is believed that the strong and stable adhesion and excellent healing performance of the APC-PVA@$ZnCl_2$ composite materials could be attributed to various synergistic effects between Zn^{2+} and hydroxyl groups, including hydrogen bonding, electrostatic attraction, and metal coordination interaction. In general, the APC-PVA@$ZnCl_2$ composite materials have strong and stable adhesion and excellent healing performance, which makes it possible to integrate the shape preservation, stability, and electrical function between the electrode and electrolyte interface, thus meeting the requirements of large deformation wearable flexible electronic materials.

In addition, the APC-PVA@$ZnCl_2$ composite material also has good self-healing characteristics, which is beneficial to realize the reuse of the material. To prove this, a deep incision was made to a piece of APC-PVA@$ZnCl_2$ composite material was cut, and it was found that with the passage of time, the incision would heal slowly. Nearly half of the incision healed after 5 h, and after 12 h, the cut APC-PVA@$ZnCl_2$ material was restored to its original state (Fig. 7a). Furthermore, the APC-PVA@$ZnCl_2$ composite material was cut in the same incision again at the same position. After the same 12 h, the new incision healed again perfectly (Fig. 7b). The above phenomenon is mainly attributed to the fact that Zn^{2+} can hybridize with hydroxyl groups on PVA through sp^3 to form coordination bonds through coordination, thus forming intermolecular forces. At the same time, PVA contains a large number of hydroxyl groups, with intramolecular forces increasing the mechanical properties of the material and making the prepared APC-PVA@$ZnCl_2$ composites have excellent self-healing properties. To further verify the self-healing performance of APC-PVA@$ZnCl_2$ composites, some bulb experiments under a closed loop were carried out. First, two strips of APC-PVA@$ZnCl_2$ ribbon composite, 5 mm thick and 70 mm long, were used as part of the closed loop. It is obvious that the small bulb can be normally lit after the power is on, and then a knife is used to cut

 This journal is © The Royal Society of Chemistry 2023

Published on 02 února 2023. Downloaded on 19.04.2026 21:13:25.

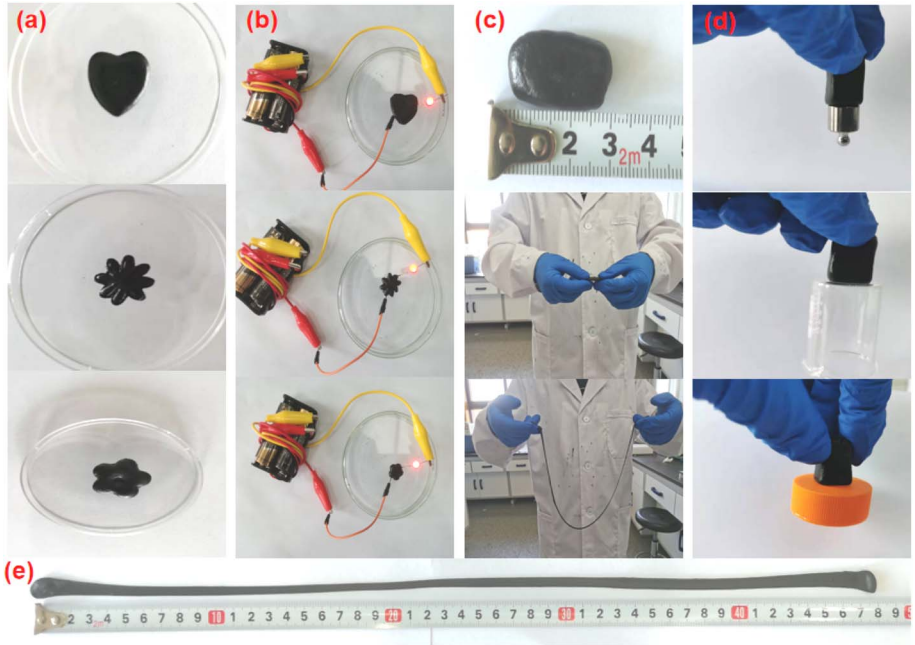

Fig. 6 (a) Digital photograph of the plasticity of APC-PVA@$ZnCl_2$ materials; (b) electrical conductivity; (c) stretchability; (d) adhesion; (e) tensile length.

a part of the belt in the closed circuit. It is found that as long as the belt structure is not completely cut off, the closed circuit can supply small bulbs with normal power. When the belt is completely cut off, the closed circuit cannot work normally, and the small bulb goes out. However, due to the self-healing function of the APC-PVA@$ZnCl_2$ composite, it was found that the incision began to heal after about 0.5 h. The result shows that once the incision began to contact, the small bulb would light again (Fig. 7b), which further proved that the APC-PVA@$ZnCl_2$ composite has excellent self-healing property. To sum up, it is firmly believed that these outstanding characteristics of the APC-PVA@$ZnCl_2$ composite material will further expand its application range.

3.3.3 Thermoelectric properties. In recent years, the Seebeck effect, which uses ions as carriers, has opened up a new way to develop high-performance thermoelectric devices.[43–46] However, the currently reported ionic thermoelectric materials are still limited by various factors, and there are some

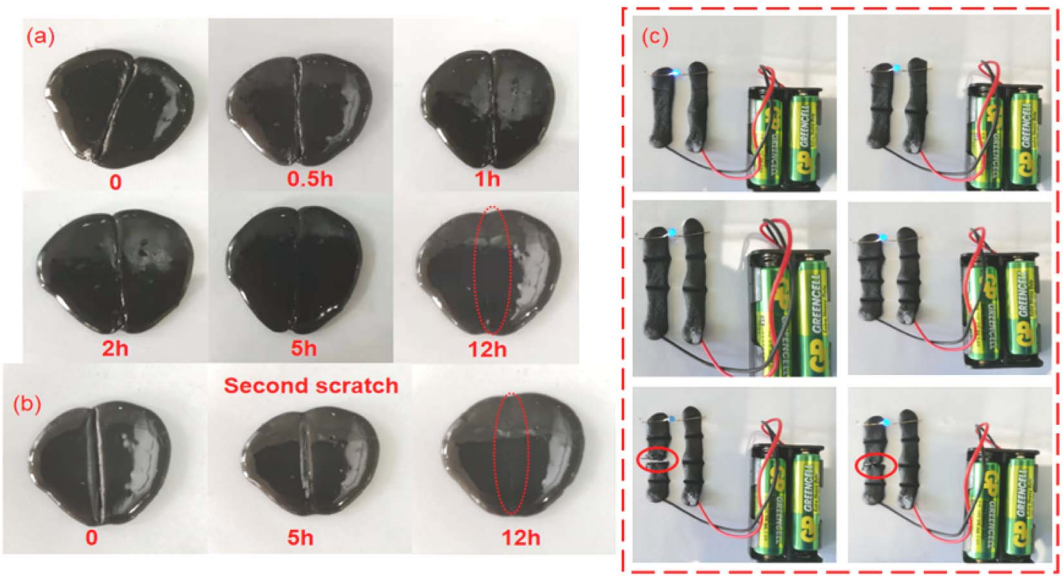

Fig. 7 (a) Self-healing experiment, (b) repeatable self-healing experiment, (c) experiment of self-healing effect on a small bulb, with on and off based on the APC-PVA@$ZnCl_2$ material.

Published on 02 února 2023. Downloaded on 19.04.2026 21:13:25.

bottlenecks that are difficult to overcome: most of the ionic thermoelectric materials are gel-containing water-soluble solutions, and the liquids are prone to evaporation or leakage, resulting in poor stability, and the ionic thermoelectric materials are mainly p-type. The choice of n-type materials with high mechanical stability and flexibility is very limited.[47] The as-obtained APC-PVA@$ZnCl_2$ material in this work shows excellent thermoelectric properties. In this work, the device in Fig. 8a is used to test the thermoelectric effect of the above materials. Fig. 8b shows the principle of thermoelectric materials, namely the Soret effect: ions move from the hot end to the cold end under the temperature gradient. The charge accumulation at the cold end caused by the diffusion difference of anion and cation is different, which will generate potential, namely thermal potential. Furthermore, it can be clearly seen from the thermoelectric test results of the material in Fig. 8c that after applying the temperature gradient, the voltage changes rapidly in the negative direction first, which is caused by the movement of free cations in the material. After a period of time, the voltage starts to change in the positive direction, and the changing trend is very slow compared with the initial stage. This is because the anion radius is larger, and the movement is slower than the cation, which is also why the cation movement appears first when the temperature field is applied. In addition, it can be seen from Fig. 8c that the number of free anions far exceeds that of cations, that is, most cations have coordinated with the chain, which is consistent with the results in the schematic diagram in Fig. 1c and also indicates that the paper-based material belongs to n-type thermoelectric material. Moreover, it is worth noting that after applying a 5 K temperature field for 4 h, 31.6 mV potential can be generated, and the Seebeck coefficient is 6.32 mV K^{-1}, which is still a high value in n-type ion thermoelectric materials.[47] More importantly, it is precisely because of this thermoelectric effect that the specific capacitance of the paper-based supercapacitor will increase to a certain extent when the temperature rises, which also confirms the test results in Fig. 4b. In general, it provides a reference for further improving and enhancing the storage capacity of energy storage devices by using the synergistic effect of the thermoelectric effect of materials and their own energy storage characteristics. To further explicitly present the measurement devices, more details can be seen in Fig. S7 of the ESI.†

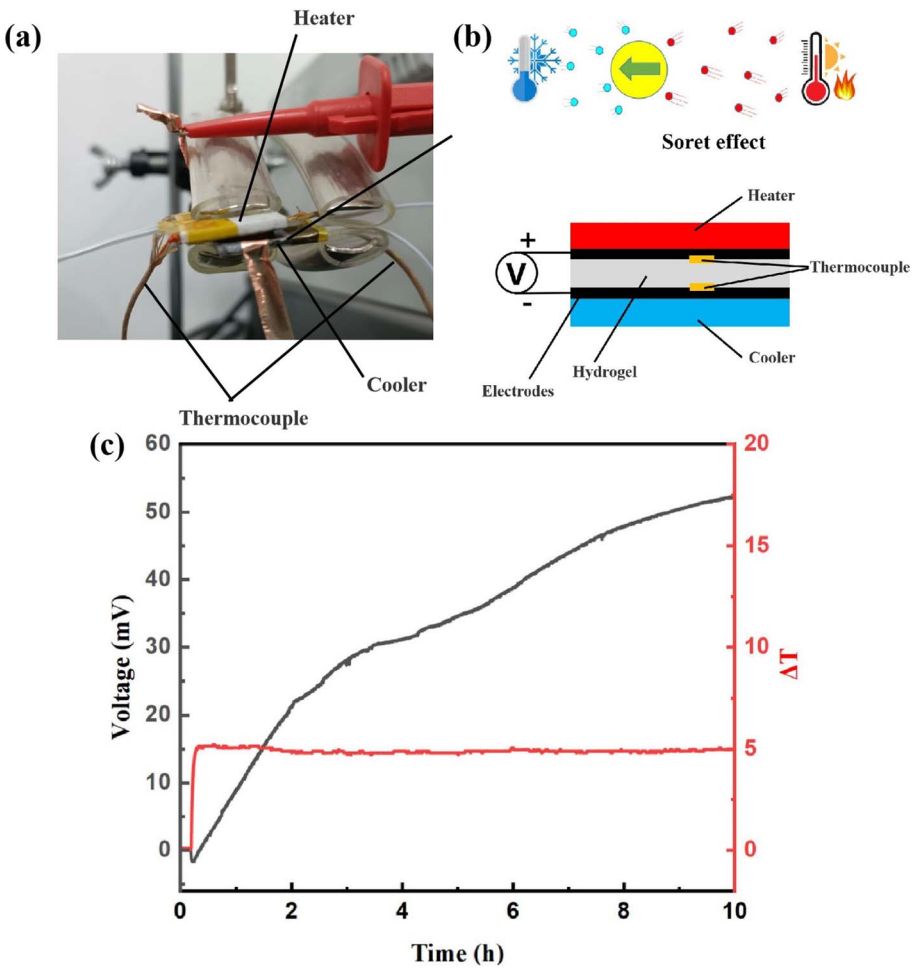

Fig. 8 Schematic diagram of (a) device and (b) principle for testing the thermoelectric effect of APC-PVA@$ZnCl_2$ materials. (c) The relationship of the change in potential of the APC-PVA@$ZnCl_2$ material with the change in temperature and time.

 This journal is © The Royal Society of Chemistry 2023

Published on 02 února 2023. Downloaded on 19.04.2026 21:13:25.

3.4. Molecular dynamics simulation

Molecular dynamics simulations were performed to gain insights into the interactions between coordinated ion and skeleton materials at the molecular level.[47,48] Three structures were built: APC-APC@$ZnCl_2$, APC-PVA@$ZnCl_2$, and PVA-PVA@$ZnCl_2$ system, respectively (Fig. 9g–i). Molecular simulation details are shown in ESI.† The mean square displacements (MSD) of Zn^{2+} in different systems are shown in Fig. 9a. It is found that the diffusion of Zn^{2+} in the APC-APC@$ZnCl_2$ system is much larger than that in the PVA-PVA@$ZnCl_2$ system. The diffusion of Zn^{2+} is enhanced when PVA is introduced and forms the APC-PVA@$ZnCl_2$ system. The coordination strength of different systems to Zn^{2+} is quantified to exhibit the binding of Zn^{2+} through radial distribution functions (RDFs), defined as the probability of finding a Zn^{2+} at distance r around O_{chain} (Fig. 9b). The significant differences in the coordination number between APC-APC@$ZnCl_2$ and PVA-PVA@$ZnCl_2$ are shown in Fig. 9b. For PVA-PVA@$ZnCl_2$, there is no obvious peak in RDFs. Correspondingly, the distinct peak of the APC-APC@$ZnCl_2$ system indicates its stronger binding to Zn^{2+}, which is favorable for the movement of Cl^-. Moreover, the binding energies of Zn^{2+} in different systems are shown in Fig. 9c. With the mixing of APC chains and PVA chains, the binding energy of Zn^{2+} to its coordination environment is 19.54 eV, which is larger than the binding energy of Zn^{2+} in the PVA-PVA@$ZnCl_2$ system, with a binding energy of 17.22 eV. It is true that for the APC-PVA@$ZnCl_2$ system, the strong Zn–O_{chain} coordinated bonding results in higher coordination numbers of Zn^{2+} around the oxygen-containing functional groups of the chain. In the APC-PVA@$ZnCl_2$ system, the Zn^{2+} can form multiple coordinations with rich oxygen functional groups (Fig. 9d), including hydroxyl (ROH), alkoxide (RO^-), and hydroxyl of water molecules. The binding of Zn^{2+} by the oxygen functional group is a crucial factor for Zn^{2+} conductivity and transport. To clarify the effect of oxygen functional group on the binding of Zn^{2+}, the charge density distribution of APC chain and PVA chain were calculated and plotted (Fig. 9e and f), and the presence of oxygen-containing functional groups makes the surface negatively charged (blue area). In other words, the blue area has strong electrostatically attractive interactions with Zn^{2+} while the red area shows a strong electrostatic rejection of Zn^{2+}. It can be clearly observed that there are more and darker blue areas on the APC chain, which indicates its stronger binding effect on Zn^{2+}. Now the theoretical calculations highlighted that the mix of APC chains and PVA chains not only enhances the toughness of the material through the strong coordination of

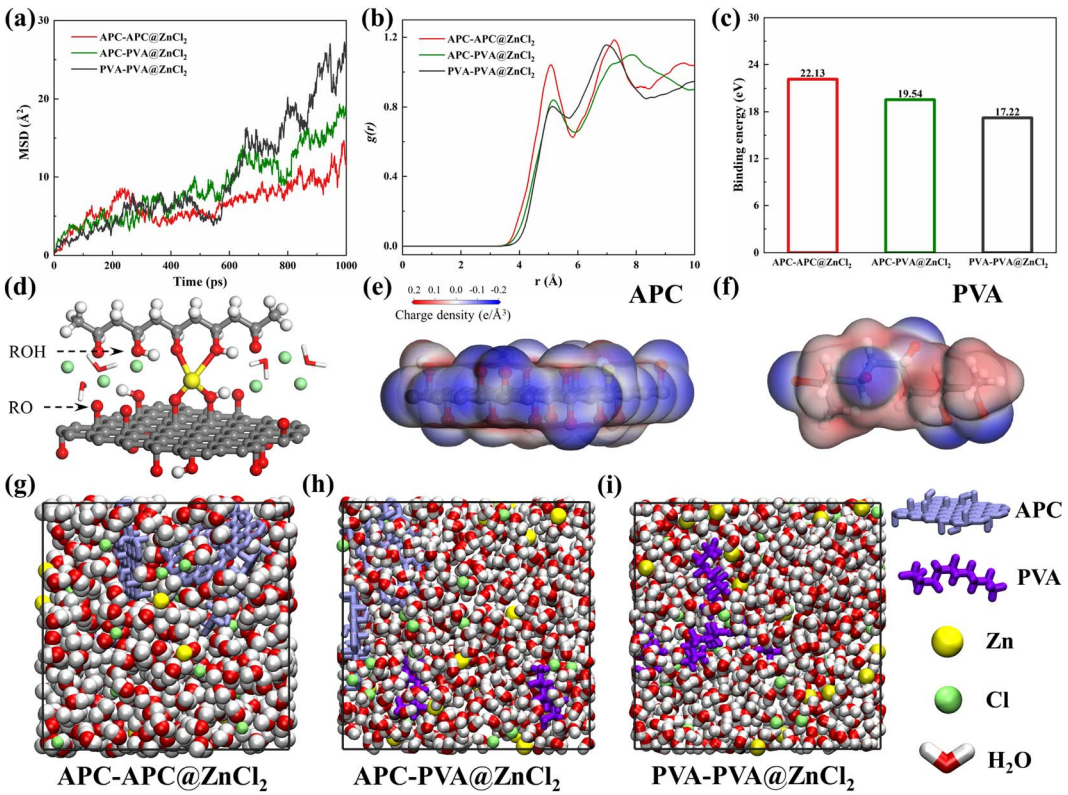

Fig. 9 Zn^{2+} conductivity and transport mechanism in carbonized paper-based materials. (a) Mean square displacement of Zn^{2+} in different systems. (b) Calculated radial distribution function of Zn–O_{chain} in different systems. (c) Binding energy of Zn^{2+} to its coordination chains in different systems. (d) Diagram showing the environment of Zn^{2+} in the APC-PVA@$ZnCl_2$ system with different oxygen atoms. C, H, O, Zn, and Cl atoms are denoted with gray, white, red, yellow, and green spheres, respectively. (e and f) Charge density distribution for (e) APC chain and (f) PVA chain, where blue area represents electron loss and red area represents electron enrichment. (g–i) Structural snapshots from molecular dynamics simulations of (g) APC-APC@$ZnCl_2$, (h) APC-PVA@$ZnCl_2$, and (i) PVA-PVA@$ZnCl_2$ systems. APC chain and PVA chain are denoted with blue and purple, respectively.

Published on 02 února 2023. Downloaded on 19.04.2026 21:13:25.

Zn^{2+} in the APC-PVA@$ZnCl_2$ system but also makes the conduction more stable by restricting the diffusion of Zn^{2+}.

4. Conclusion

In conclusion, a simple and effective method has been successfully designed to construct a kind of carbonized paper-based integrated multi-functional composites. Due to the light and porous properties of paper-based materials and the interaction between nano-fiber, PVA, and $ZnCl_2$, the as-fabricated integrated paper-based supercapacitor exhibits the following merits: (1) due to the formation of coordination bonds and hydrogen bonds between PVA/$ZnCl_2$ and nano-fiber, the integrated paper-based supercapacitor shows excellent comprehensive mechanical properties. (2) PVA/$ZnCl_2$ acts as a gel electrolyte, endowing the integrated paper-based energy storage device with ultra-high specific capacitance, specific energy, and specific power density. (3) Due to the introduction of PVA/$ZnCl_2$, the integrated paper-based supercapacitor shows excellent electrochemical energy storage characteristics at different ambient temperatures, such as high, normal, and low temperatures. (4) The constructed integrated paper-based supercapacitor shows excellent plasticity, tensile strength (elongation can reach 2400–2500%), adhesion, and self-healing. (5) The integrated paper-based supercapacitor can also act as a sensor, showing good stability and high sensitivity in monitoring human movements. (6) The constructed integrated paper-based supercapacitor shows a superior thermoelectric effect. Moreover, the results of molecular dynamics simulation further support the above results. In summary, this research work provides a new idea for the multi-functional and integrated high-efficiency development, application, and recycling of green biomass materials from the perspective of experiment and theory.

Conflicts of interest

There are no conflicts to declare.

Acknowledgements

This work was supported by funds from the National Natural Science Foundation of China (22078184 and 52006130), China Postdoctoral Science Foundation (2019M653853XB), Natural science advance research foundation of Shaanxi University of Science and Technology (2018QNBJ-03), the Youth Science and Technology Nova Program of Shaanxi Province (2021KJXX-07), and the Joint Research Funds of Department of Science and Technology of Shaanxi Province and Northwestern Polytechnical University (2020GXLH-Z-025).

References

1 A. K. Ettinger, C. J. Chamberlain and E. M. Wolkovich, *Nat. Clim. Change*, 2022, **12**(4), 305–307.
2 A. G. Olabi and M. A. Abdelkareem, *Renewable Sustainable Energy Rev.*, 2022, **158**, 112111.
3 C. Xiong, T. Wang, Z. Zhao and Y. Ni, *Smart Mater.*, 2023, **4**(2), e1158.
4 M. Wu, W. Zheng, X. Hu, F. Zhan, Q. He, H. Wang, Q. Zhang and L. Chen, *Small*, 2022, **18**(50), 2205101.
5 C. Xiong, T. Wang, Y. Zhang, M. Zhu and Y. Ni, *Nano Res.*, 2022, **15**(8), 7506–7532.
6 F. Wang, Y. Liu, H. Wei, T. Li, X. Xiong, S. Wei, F. Ren and A. A. Volinsky, *Rare Met.*, 2021, **40**, 448–470.
7 M. Peng, L. Wang, L. Li, Z. Peng, X. Tang, T. Hu, K. Yuan and Y. Chen, *eScience*, 2021, **1**, 83–90.
8 C. Xiong, T. Wang, Y. Zhang, B. Li, Q. Han, D. Li and Y. Ni, *Int. J. Hydrogen Energy*, 2022, **47**(4), 2389–2398.
9 J. Chen, W. Xu, H. Wang, X. Ren, F. Zhan, Q. He, H. Wang and L. Chen, *J. Mater. Chem. A*, 2022, **10**, 21197.
10 C. Xiong, W. Dang, S. Nie, C. Qin, D. Li, L. Dai, M. Shen, Y. Xu and Y. Ni, *Cellulose*, 2021, **28**(3), 1455–1468.
11 J. Huang, S. Han, J. Zhu, Q. Wu, H. Chen, A. Chen, J. Zhang, B. Huang, X. Yang and L. Guan, *Adv. Funct. Mater.*, 2022, **32**(35), 2205708.
12 C. Xiong, Y. Zhang and Y. Ni, *J. Power Sources*, 2023, **560**, 232698.
13 L. Mao, X. Zhao, Y. Li and L. Chen, *J. Colloid Interface Sci.*, 2022, **624**, 482.
14 C. Xiong, B. Li, H. Liu, W. Zhao, C. Duan, H. Wu and Y. Ni, *J. Mater. Chem. A*, 2020, **8**(21), 10898–10908.
15 J. Chen, D. Shi, Z. Yang, W. Dong and M. Chen, *J. Power Sources*, 2022, **532**, 231326.
16 M. Zhou, S. Yan, Q. Wang, M. Tan, D. Wang, Z. Yu, S. Luo, Y. Zhang and X. Liu, *Rare Metals*, 2022, **41**(7), 2280–2291.
17 J. Guo, J. Xu, X. Xiao, L. Dai, C. Zhang and K. Huo, *Green Chem.*, 2022, **24**, 8827–8839.
18 C. Xiong, C. Zheng, B. Li and Y. Ni, *Ind. Crops Prod.*, 2022, **178**, 114565.
19 P. B. Naik, P. Yadav, R. Nagaraj, R. Puttaswamy, H. K. Beere, U. N. Maiti, C. Mondal, N. S. Kotrappanavar and D. Ghosh, *ACS Sustainable Chem. Eng.*, 2022, **10**(4), 1471–1481.
20 C. Xiong, M. Li, Q. Han, W. Zhao, L. Dai and Y. Ni, *J. Mater. Sci. Technol.*, 2022, **97**, 190–200.
21 W. Kang, L. Zeng, X. Liu, H. He, X. Li, W. Zhang, P. S. Lee, Q. Wang and C. Zhang, *Electrochem. Energy Rev.*, 2022, **5**(3), 8.
22 M. Shen, W. Hu, C. Duan, J. Li, S. Ding, L. Zhang, J. Zhu and Y. Ni, *J. Colloid Interface Sci.*, 2023, **629**, 778–785.
23 Y. Sun, Y. Yuan, X. Geng, C. Han, S. Lu, I. Mitrovic, L. Yang, P. Song and C. Zhao, *Carbon*, 2022, **199**, 224–232.
24 I. Alali and R. Mokaya, *Energy Environ. Sci.*, 2022, **15**(11), 4710–4724.
25 Z. Qu, X. Zhang, R. Huang, S. Wu, R. Chen, F. Wu and L. Li, *Nano Lett.*, 2022, **22**(10), 4115–4123.
26 C. Xiong, B. Li, C. Duan, L. Dai, S. Nie, C. Qin, Y. Xu and Y. Ni, *Chem. Eng. J.*, 2021, **418**, 129518.
27 D. Gogoi, P. Makkar, M. R. Das and N. N. Ghosh, *ACS Appl. Electron. Mater.*, 2022, **4**(2), 795–806.
28 S. Long, Y. Feng, F. He, J. Zhao, T. Bai, H. Lin, W. Cai, C. Mao, Y. Chen, L. Gan, J. Liu, M. Ye, X. Zeng and M. Long, *Nano Energy*, 2021, **85**, 105973.

 This journal is © The Royal Society of Chemistry 2023

Published on 02 února 2023. Downloaded on 19.04.2026 21:13:25.

29 Y. Hu, Z. Chen, H. Zhuo, L. Zhong, X. Peng and R. Sun, *Adv. Funct. Mater.*, 2019, **29**(44), 1904472.
30 Q. Ding, X. Xu, Y. Yue, C. Mei, C. Huang, S. Jiang, Q. Wu and J. Han, *ACS Appl. Mater. Interfaces*, 2018, **10**(33), 27987–28002.
31 J. Han, H. Wang, Y. Yue, C. Mei, J. Chen, C. Huang, Q. Wu and X. Xu, *Carbon*, 2019, **149**, 1–18.
32 M. Darabi, A. Khosrozadeh, Y. Wang, N. Ashammakhi, H. Alem, A. Erdem, Q. Chang, K. Xu, Y. Liu, G. Luo, A. Khademhosseini and M. Xing, *Adv. Sci.*, 2020, **7**(21), 1902740.
33 B. Chen, Q. Chen, S. Xiao, J. Feng, X. Zhang and T. Wang, *Sci. Adv.*, 2021, **7**(48), eabi7233.
34 Y. Heo, J. Lee, S. Kim, S. Mun, S. Lee and S. Park, *ACS Appl. Mater. Interfaces*, 2022, **14**(37), 42671–42682.
35 H. Peng, S. Huang, D. N. Tranca, F. Richard, W. Baaziz, X. Zhuang, P. Samori and A. Ciesielski, *ACS Nano*, 2022, **15**(11), 18580–18589.
36 D. Mudusu, K. R. Nandanapalli, G. D. Moon and S. Lee, *Nano Energy*, 2021, **88**, 106274.
37 A. M. Patil, N. R. Chodankar, E. Jung, S. Roy, D. P. Dubal, G. Guan, Y. K. Han and S. C. Jun, *J. Mater. Chem. A*, 2021, **9**(46), 26135–26148.
38 F. Wang, J. Cheong, J. Lee, J. Ahn, G. Duan, H. Chen, Q. Zhang, I. D. Kim and S. Jiang, *Adv. Funct. Mater.*, 2021, **31**(31), 2101077.
39 Q. Liu, A. Zhao, X. He, Q. Li, J. Sun, Z. Lei and Z. Liu, *Adv. Funct. Mater.*, 2021, **31**(22), 2010944.
40 H. Shi, S. Chen, W. Shi, Z. Peng, J. Li, Z. Liu, G. Zhang and L. Liu, *J. Mater. Chem. A*, 2021, **9**(31), 16852–16859.
41 Z. Peng, J. Huang, Q. He, L. Tan and Y. Chen, *J. Mater. Chem. A*, 2021, **9**(7), 4273–4280.
42 C. Yu, H. Xu, Y. Gong, R. Chen, Z. Hui, X. Zhao, Y. Sun, Q. Chen, J. Zhou and W. Ji, *Research*, 2021, **2021**, 6742715.
43 J. Xie, M. Han, X. Zeng, D. Mao, H. Li, X. Zeng, R. Liu, L. Ren, R. Sun and J. Xu, *Chem. Eng. J.*, 2022, **435**(3), 135172.
44 S. Liu, Y. Yang, H. Huang, J. Zheng, G. Liu, T. H. To and B. Huang, *Sci. Adv.*, 2022, **8**(1), eabj3019.
45 E. H. Suh, M. K. Jeong, K. Lee, W. Jeong, Y. J. Jeong, I. H. Jung and J. Jang, *Adv. Funct. Mater.*, 2022, **32**(51), 2207886.
46 O. Zapata-Arteaga, S. Marina, G. Zuo, K. Xu, B. Dorling, L. A. Perez, J. S. Reparaz, J. Martin, M. Kemerink and M. Campoy-Quiles, *Adv. Energy Mater.*, 2022, **12**(19), 2104076.
47 C. Chi, M. An, X. Qi, Y. Li, R. Zhang, G. Liu, C. Lin, H. Huang, H. Dang and B. Demir, *Nat. Commun.*, 2022, **13**(1), 221.
48 W. Zhou, Y. Wu, H. Huang, M. Zhang, X. Sun, Z. Wang, F. Zhao, H. Zhang, T. Xie and M. An, *Renewable Sustainable Energy Rev.*, 2022, **168**, 112767.